Supporting Information For:

Aqueous Photochemistry of Glyoxylic Acid

DOI: 10.1021/acs.jpca.6b00225

Publication Date (Web): May 18, 2016

*Alexis J. Eugene, Sha-Sha Xia, and Marcelo I. Guzman**

Department of Chemistry, University of Kentucky, Lexington, Kentucky 40506, Unites States

*Corresponding author's email: marcelo.guzman@uky.edu

The Journal of Physical Chemistry A

Content **Pages**

Preparation of experiments and controls S2-S3
Photochemical experiments and thermal treatment of photolyzed samples S4-S5
Analysis of products S5-S9
Evaluation of Beer's law S9-S10
Assignment of an absorbing tail to glyoxylic acid. S10-S11
Apparent quantum yields of CO_2 and CO production S12
Quasi-steady state glyoxal production under 1 atm O_2(g) or N_2(g). S12-S13
Apparent quantum yields of formic, oxalic, and tartaric acids S13-S14

Figures
Figure S1. Absorbance at the end of stage II S9
Figure S2. UV-visible spectra of glyoxylic acid at variable concentration S11
Figure S3. ^{13}C NMR spectrum of reagent S11
Figure S4. Apparent quantum yields of CO_2 and CO production S12
Figure S5. Quasi-steady state glyoxal production S12
Figure S6. Apparent quantum yields of formic, oxalic, and tartaric acids S14

Tables
Table S1. Experiments and controls S4

References S15-S17

Detailed Experimental Section

Preparation of experiments and controls. The concentration range for glyoxylic acid used is bracketed by the water to sulfate ratio found in remote and urban aerosols.[1] Considering the deliquescence curve of an ammonium bisulfate solution[2,3] at 50 % relative humidity (RH), fine arctic aerosol particles contain 0.6 g of H_2O/g of SO_4^{2-} or up to [glyoxylic acid] ≈ 250 mM[4] under very acidic conditions,[1] while polluted city environments such as Tokyo can exceed this concentration by 3 times.[5] Therefore, *ca.* 250 mM glyoxylic acid (Sigma-Aldrich, 52.1 wt. % in H_2O) solutions were prepared daily in water (Elga Purelab flex, 18.2 MΩ cm^{-1}). Additional experiments studied the effect of glyoxylic acid concentration covering the range 5-250 mM. "

Even though related studies employed glyoxylic acid monohydrate (Fluka, 97%) of lower purity without further purification,[6,7] we discarded the use of the monohydrate (98%) and selected the aqueous solution of higher purity for the work. The selection of the aqueous reagent considered the evaluation of impurities present in glyoxylic acid monohydrate (Sigma Aldrich, 98%) before and after purification by two methods: 1) Purification of the solid by gently warming the monohydrate to 40 °C under vacuum at 17 mTorr was performed for 12 h, as described elsewhere;[8] and 2) recrystallization of the monohydrate in chloroform (Fisher Optima, LC-MS grade) recovering a 55 wt. % as white crystals. However, even after both purification procedures, the purity of the reagent did not appear to be larger than for the aqueous reagent chosen for this work, as revealed using the multiple techniques described in the experimental section. For example, ion chromatography showed that the aqueous reagent (glyoxylic acid, 52.1 wt. %) used for the work was appropriately selected.

The solution of glyoxylic acid was doped with the most abundant inorganic electrolytes found in seawater,[9] which form sea spray aerosols. The electrolytes included [Na^+] = 468 mM, [Cl^-] =

545 mM and $[SO_4^{2-}]$ = 28.2 mM prepared from NaCl (Fisher, 99 %), Na_2SO_4 (Fisher, 99 %) and HCl (EMD, 38 %). This mixture does not contain NH_4^+ in order to focus the work on the effects caused by photoirradiation instead of reiterating the reported catalysis by ammonium[10] that can lead to decarboxylation.[1,11,12] After adjusting the pH of the glyoxylic acid solution to 1.0 with [HCl] = 2.0 M, 180 mL were transferred to a customized fused silica photoreactor (220 mL capacity) provided with a jacket for temperature control at 298 K (Thermo Scientific A25 circulating bath), magnetic stirring, and a port for sampling gases through a septum. The sealed reactor underwent continuous sparging (unless indicated otherwise) with 100 mL min^{-1} air (Scott-Gross, UHP) starting 30 minutes before photolysis. Experiments are performed under 1 atm air and the conditions of ionic strength, temperatures and photon flux are chosen to simulate those encountered by nascent sea spray aerosols mixing with pollution at coastal regions.

Control experiments (Table S1) were designed to study the effect of inorganic electrolytes and $[O_2(aq)]$ on the photoreaction of glyoxylic acid. In more detail Table S1 indicates which gas was used and if electrolytes were not present in the controls: Control A under 1 atm $N_2(g)$ (Scott-Gross, UHP), control B under 1 atm $O_2(g)$ (Scott-Gross, UHP), control C without electrolytes, control D without electrolytes under 1 atm $N_2(g)$, and control E without electrolytes under 1 atm $O_2(g)$. From Henry's law (K_H = 1.28 × 10^{-3} M atm^{-1} for O_2 at 298 K),[13] $[O_2(aq)]_{1\ atm\ air}$ = 0.26 mM and $[O_2(aq)]_{1\ atm\ O_2}$ = 1.24 mM.

Table S1. Experiments and controls to investigate the photoreaction of glyoxylic acid

	Conditions				
	$h\nu$	Electrolytes	Atmosphere		
			Air	N_2	O_2
Experiment	✓	✓	✓		
Control A	✓	✓		✓	
Control B	✓	✓			✓
Control C	✓		✓		
Control D	✓			✓	
Control E	✓				✓
Control F		✓	✓		

Key: $h\nu$ indicates the presence of light ($\lambda \geq 305$ nm). Electrolytes include Na^+, Cl^- and SO_4^{2-}.

Photochemical experiments and thermal treatment of photolyzed samples. The photochemical setup (Newport) employed was previously described[14] and includes a 1 kW high-pressure Xe-Hg lamp, a water filter to remove infrared radiation, and a cut-off filter for wavelength $\lambda \geq 305$ nm that provides actinic radiation in the solar window. During the first stage of processing (Stage I in Scheme 1), samples of the experiment and controls (Table S1) were irradiated for 8 h and 5 mL aliquots were withdrawn from the reactor at 0, 0.5, 1, 2, 3, 4, 5, 6, 7, and 8 h. A 30% of the aliquot was immediately frozen at 253 K and stored in the dark for later analyses by IC-MS, UHPLC-MS, and NMR spectroscopy. The remaining 3.5 mL of sample was transferred to a Suprasil cuvette (Starna Cells, 10-mm optical path length) to monitor its aging (Stage II in Scheme 1) in the dark

by UV-visible spectroscopy for 15 h at 298 K followed by 9 h at 323 K. About 130 mL of the remaining aged-photolyzed sample was stored in the dark for 24 h and then re-photolyzed (Stage III in Scheme 1). Re-photolyzed samples underwent a second aging process in the dark monitored by UV-visible spectroscopy (Stage IV in Scheme 1).

Analysis of products. Samples were analyzed by 1) UV-visible spectroscopy; 2) ion chromatography (IC) equipped with a conductivity detector and a mass spectrometer (MS) interfaced with an electrospray ionization (ESI) probe (IC-MS); 3) UHPLC-MS; 4) Fourier transform infrared spectroscopy (FTIR) for gases; and 5) ^{1}H and ^{13}C NMR experiments. Data from all these methods is reported as the average of duplicate experiments with error bars corresponding to one standard deviation. The competition between homolytic cleavage[15] and hydrogen abstraction[16,17] resulting from excited triplet state glyoxylic acid could be indirectly assessed from the abundance of products generated by each channel.

UV-visible spectra ($190 \leq \lambda \leq 750$ nm) of initial and irradiated samples were recorded immediately after sampling with an Evolution 220 scanning spectrophotometer (Thermo Scientific) equipped with a temperature control multi-cell holder (Thermo Scientific, SPE 8 W). In addition, spectra were recorded during the aging processing every 30 min. Actual initial concentrations of glyoxylic acid in the solutions were registered from total absorbance readings using Beer's Law and the molar absorptivity of glyoxylic acid in water at $\lambda = 240$ nm:[18] $\varepsilon_{GA} = 11.6$ M^{-1} cm^{-1}. An aged sample from the end of stage II (Scheme I) was placed in a 10 mm optical path micro fluorometer cell (Starna) for registering the fluorescence emission spectra at 298 K using a FluroMax-4 fluorimeter (Horiba Scientific) and FluorEssence software. The excitation wavelength (λ_{exc}) was varied over the range 350-400 nm to record emission spectra up to 800 nm. A single

accumulation with 0.1 s integration time and 1 nm step size was employed. A sample with 11.8 mM glyoxal (the actual amount quantified at the end of Stage II) with the same electrolyte composition as the experiment was aged for comparison. A solution of electrolytes (no organics) was used as a blank to subtract out the water Raman peak from each spectrum.

Samples for ion chromatography in the low millimolar range of glyoxylic acid were obtained by dilution (0 to 50 times) of the photolyzed aliquots with water, depending on $[\text{glyoxylic acid}]_0$. Chromatographic samples were immediately injected with an autosampler (Dionex AS) in an IC (Dionex ICS-2000) provided with an IonPack AS11-HC (2 mm) analytical column and a conductivity detector. An ESI probe interfaced the output of the conductivity detector to a mass spectrometer (Thermo Scientific, MSQ Plus) as described before.[14] The ESI-MS operates in negative ion mode for the m/z range 50-500 amu at 70 psi N_2 nebulizing gas, 450 °C, 1.9 kV needle voltage, and 50 V cone voltage, unless indicated otherwise. Tartaric and oxalic acids were detected as the mono-anions at *m/z* 149.01 and 88.99, respectively. Sodium oxalate (Alfa Aesar, 99.9 %) and L-(+)-tartaric acid (Sigma Aldrich, 99.7%) were used as standards for the quantification.

An Accela (Thermo Fisher Scientific) UHPLC with a 1250 quaternary delivery pump and a MS detector (MSQ Plus) was employed for the analysis of carbonyls after derivatization with freshly prepared 2,4-dinitrophenylhydrazine (DNPH, Sigma Aldrich, HPLC grade). For the general identification of carbonyls, 26 µL of photolyzed sample were diluted to a volume of 5 mL, mixed with 5 mL [DNPH] = 25.02 mM dissolved in acetonitrile with 4 % H_2SO_4, and incubated at 20 °C during 1 h. The derivatized samples were mixed with an equal volume of methanol (Fisher Optima, LC-MS grade) and injected (25 µL) with an Accela autosampler into a reversed-phase column (Hypersil GOLD C18 column 1.9 µm, 50×2.1 mm, Thermo Scientific) for separation of hydrazones. The carbonyls in the mixture were compared to those of standard hydrazones for

glyoxylic acid, formaldehyde (Mallinckrodt, 37.2 %), and glyoxal (Sigma Aldrich, 38.5 wt. %), which were observed by mass spectrometry at m/z 253.02, 209.03, and 417.05, respectively.

Chromatographic separation at a constant flow rate of 800 μL min^{-1} from 0 to 1 min was isocratic with 70 % (solvent A) 0.10 mM formic acid (Fisher Optima, LC-MS grade) in ultrapure water (18.2 MΩ cm) and 30 % (solvent B) 0.10 mM formic acid in methanol (Fisher Optima, LC-MS grade). Gradient elution from 1 to 7 min reached a 45:55 ratio of solvents A:B and remained isocratic from 7 to 9 min. The UHPLC was interfaced to the MS by an ESI probe (1.9 kV needle voltage, 350 °C probe temperature, 50 V cone voltage, and 70 psi N_2 nebulizing gas) to detect negative ions. Excalibur software was used to control the UHPLC-MS system. Gaussian functions were employed to fit the data reported. A calibration curve made with glyoxal was used to correlate extracted ion chromatogram peak area with dihydrazone concentration in samples. Formaldehyde production in the photolyzed was discarded by this analysis as well as by NMR and FTIR methods described below. The careful quantification of glyoxylic acid was only possible after modifying the above protocol by diluting the samples 2.25×10^4 times ($pH_{final} = 2$) prior to DNPH addition.

NMR (Varian 600 MHz) spectra were recorded at 298 K using 5-mm NMR tubes (Wilmad) with 540 μL of sample spiked with 60 μL of 121.44 mM 3-(trimethylsilyl)-1-propanesulfonic acid sodium salt (DSS, Aldrich, 97 %) internal standard in D_2O (Cambridge Isotope Laboratories, 99.9 %) for field-frequency lock, using a 90° pulse length for ^{13}C NMR. Although ^1H NMR is not the preferred choice of analysis because most products of interest appear under the water peak, the production of formic acid could be quantified by this method. For this purpose, the samples described above were spiked with 10 μL of 7.47 mM gadolinium (III) chloride (Aldrich, 99.999 %) in D_2O to shorten T_1 relaxation times. ^1H NMR spectra were recorded using a water suppression

enhanced through T_1 effects solvent suppression (WET) method. Equation 1 was used to calculate [formic acid] by comparison to the area of DSS internal standard:

$$[\text{formic acid}] = \frac{[\text{DSS}] \times (\text{area of formic acid})}{(\text{area of DSS})} \times \frac{9}{1} \quad (1)$$

where the area of formic acid is obtained by integrating the peak at δ 8.241 (s, 1H), which is only shifted -0.016 ppm relative to the spectral database value,[19] the area of DSS corresponds to the strong singlet at δ 0.000 (s, 9H), and the factor 9/1 represents the ratio of hydrogen atoms in DSS to formic acid.

For the analysis of evolving gases, the same experimental conditions were used with the exception that the sealed reactor filled with air was not continuously sparged. Aliquots of 500 µL of the reactor headspace were withdrawn through the septum with a syringe provided with a stainless steel needle for analysis in a 2.4 m path length infrared gas cell with ZnSe windows (PIKE) and a capacity of 100 cm^3. The cell was mounted in an iZ10 FT-IR module connected to an infrared microscope (Thermo Scientific Nicolet iN10). Equilibration of gases in the cell during 30 min was allowed prior to scanning. The optics were continuously purged with N_2(g) while recording 128 scans of background and sample spectra in absorption mode with 1 cm^{-1} resolution over the range 500-4000 cm^{-1}. For the quantification of CO_2 and CO the respective R-branch, centered at 2361 and 2176 cm^{-1}, were baseline-corrected and integrated in the absorbance spectra. For calibration purposes, samples of known [CO_2(g)] and [CO(g)] were generated during the photodecarboxylation of 25 mM aqueous solutions of phenylglyoxylic acid (Alfa Aesar, 99.9 %) at pH 1.0[20,21], and the photodecarbonylation of 10 mM solutions of 1,3-diphenyl-2-propanone (Aldrich, 99.7 %) in benzene[22,23] (EMD, Omnisolv, 99.7 %), respectively. The same liquid to headspace volume ratio of experiments was kept for these analyses providing concentrations in molar units relative to the liquid volume.

Evaluation of Beer's law. Figure S1A presents the absorption changes and linear regression at selected wavelengths (λ = 280, 295, 320, 350, 420, 450 and 500 nm) for the same experiment in Figure 1 (after stage II) upon successive dilutions with water by 1, 2, 4, and 10 times. For each monochromatic radiation Beer's law is followed well only for the UV and shorter visible range (λ ≲ 400 nm). However, for λ > 400 nm the absorptivity decays monotonically resulting in a nonlinear behavior.

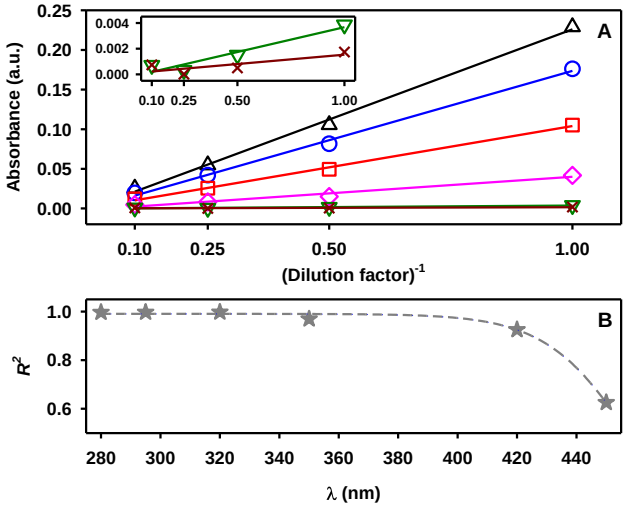

Figure S1. (A) Absorbance of experiment with glyoxylic acid in Figure 1 at the end of stage II (Scheme 1 and Figure 2) *vs.* the reciprocal of dilution factor at wavelength (λ): (black Δ) 280, (blue ○) 295 nm, (red □) 320, (pink ◊) 350, (green ▽) 420, and (dark red ×) 450 nm. (B) Coefficient of determination (R^2) for linear regression data in part A.

Figure S1B shows large changes in the coefficient of determination (R^2) of the linear regressions in part A. The progressive loss of linearity at higher λ is due to typical instrumental limitations. Therefore, we conclude that Beer's law was obeyed between 280 and 500 nm within the experimental accuracy. The complex mixture after stage II represents the low molecular weight fraction of organic matter found in atmospheric waters, which affects the optical properties of

particulate matter. The multiple functional groups present in the photolyzed and thermally aged samples behave as absorbing species but can also scatter light in the presence of electrolytes.[12,24] This issue should be the focus of future combined modeling and experimental efforts, accounting for the fact that the composition of organic aerosols varies with geographical location, altitude, and the time of day.[12,24]

Assignment of an absorbing tail to glyoxylic acid. Figure S2 shows how the absorbance of glyoxylic acid solutions in the presence of electrolytes increases with concentration. At low concentrations, there is little light absorbed above λ = 250 nm. However, at the concentrations used in this study, the C=O absorption band for the characteristic n→π* transition (λ_{max} = 276 nm) grows significantly following a perfect linear trend (see inset of Figure S2). If any impurity with a chromophore absorbing at λ = 305 nm would be present in the sample, its tail in the region of maximum absorption for glyoxylic acid (λ_{max} = 276 nm) should have produced a larger deviation from the practically perfect linear fitting with correlation coefficient R^2 = 0.9998. Because the latter is not the case, the data in Figure S2 strongly supports the assignment of the absorbing tail to glyoxylic acid. This band has a large tail that extends well into the tropospheric actinic window. The hydration equilibrium of glyoxylic acid demands that 833 μM of aldehyde form is available to absorb light in a 250 mM total solution.

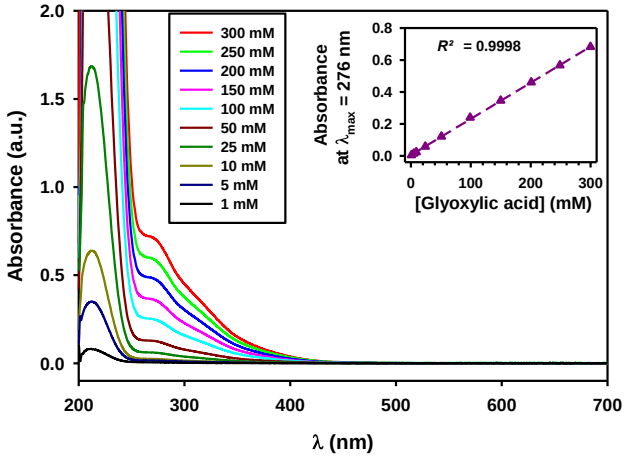

Figure S2. UV-visible spectra of [glyoxylic acid] = 1, 5, 10, 25, 50, 100, 150, 200, 250, and 300 mM in the presence of electrolytes. Inset: Absorbance at λ_{max} = 276 nm vs. [glyoxylic acid] fitted with a straight line with correlation coefficient R^2 = 0.9998.

Figure S3 presents the ^{13}C NMR spectrum for the reagent used in this study that confirms no other chromophore is present. Only the signals for the gem-diol (–C(OH)$_2$) group at δ 88.89 ppm and the carboxylic acid group (–COOH) at δ 175.90 of glyoxylic acid are registered in the spectrum.

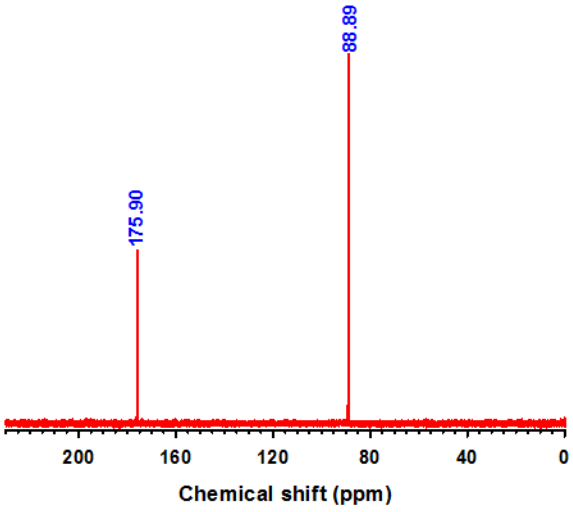

Figure S3. ^{13}C NMR spectrum of glyoxylic acid reagent as received. Chemical shifts are assigned by comparison to the value for glyoxylic acid in Figure 6 of the main text.

Apparent quantum yields of CO_2 and CO production under 1 atm O_2(g) or N_2(g). Figure S4 shows the apparent quantum yields Φ_{CO_2} and Φ_{CO} as well as their ratio, which is discussed in the main text.

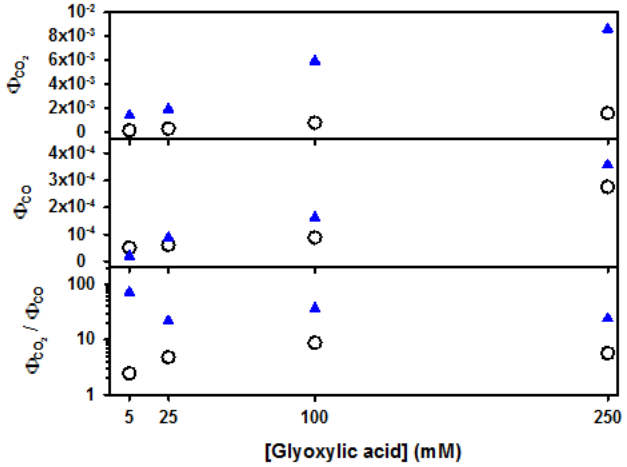

Figure S4. Apparent quantum yields of formation for (top panel) CO_2(g) and (center panel) CO(g) vs initial $[\text{glyoxylic acid}]_0$ during 2 h photolysis ($\lambda \geq 305$ nm) in electrolytes under (black ○) 1 atm N_2(g) or (blue ▲) 1 atm O_2(g).

Quasi-steady state glyoxal production under 1 atm O_2(g) or N_2(g). Figure S5 presents the quasi-steady state glyoxal production obtained by extrapolating the concentration of glyoxal to infinite time for experiments in the presence or absence of dissolved O_2.

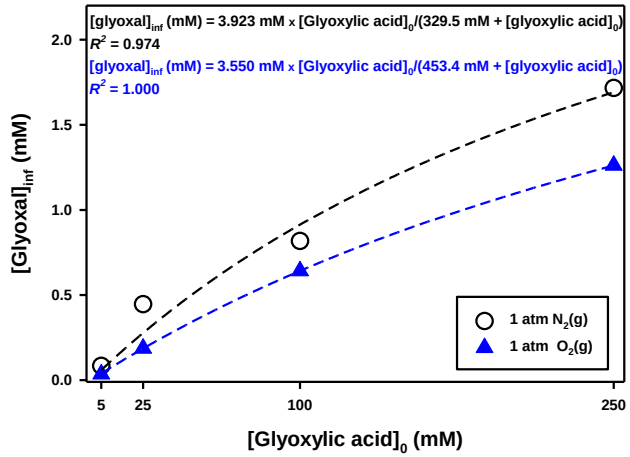

Figure S5. Quasi-steady state glyoxal production obtained as time $\rightarrow \infty$ ($[\text{glyoxal}]_{inf}$) vs initial $[\text{glyoxylic acid}]_0$ during 8 h photolysis ($\lambda \geq 305$ nm) in electrolytes under (black ○) 1 atm N_2(g) or (blue ▲) 1 atm O_2(g).

It is interesting to examine if the glyoxal generated could contribute to the observed photochemistry by absorbing light. However, glyoxal is largely hydrated in water (overall hydration constant: K_{hyd} = 7.22 × 10^4 - 2.2 × 10^5)[25-27] forming a tetrol. A rough estimate for the amount of glyoxal monohydrate (the intermediate form with one C=O group) of 13.85 ppm is obtained using lower value for K_{hyd}. Therefore, for the stable [glyoxal] = 2.02 mM during stage I, the [monocarbonyl] ≤ 28 nM. If a similar molar absorptivity to glyoxylic acid is considered for glyoxal in the experiment of Figure 7, then the contribution of glyoxal to the total absorbance is 2.8 × 10^4 times smaller than for glyoxylic acid. The number resulting from the [glyoxal monohydrate] estimated suggests an insignificant contribution of glyoxal to the photochemistry observed. For the hypothetical case of photon absorption by glyoxal in our system, we would still expect identical products to the ones observed, which would originate by analogous reactions to those displayed for glyoxylic acid in Scheme 2.

Apparent quantum yields of formic acid, oxalic acid, and tartaric acid production under 1 atm O_2(g) or N_2(g). Figure S6A-B shows the enhanced apparent quantum yields for formic and oxalic acids in the presence of dissolved oxygen. In addition to the reactions presented in the main text, the following O_2(aq) dependent pathways for formic acid production are suggested: 1) addition of dissolved oxygen to the formyl radical •C(H)=O, and a subsequent Russell type disproportionation that generates the formylperoxyl radical in water, as proposed to explain the generation of singlet oxygen ($^1\Delta_g$) during glyoxal oxidation,[28] and 2) addition of HO_2 to the formyl radical to form unstable performic acid, which immediately decays into formic acid or CO_2/H_2O as observed in the gas phase.[29,30] Therefore, the proposed reactions of formyl radical with either O_2(aq) or HO_2 producing HCOOH or CO_2 depend on the diradical. The ratio of quantum yields

for formic acid formation under 1 atm O_2(g) to 1 atm N_2(g) is ~6 for [glyoxylic acid]$_0$ = 5 and ~3 for [glyoxylic acid]$_0$ = 250 mM. Therefore, reaction R5 is favored when there are fewer glyoxylic acid molecules available to scavenge the formyloxyl radical HOOC$^{\bullet}$. In agreement, oxalic acid production from G$^{\cdot}$ is also enhanced in the presence of O_2(aq), which is eliminated as HO_2 in reaction R9 (Scheme 1).

Finally, the quantum yield of tartaric acid (Figure S6C) is only enhanced due to the presence of O_2(aq) for [glyoxylic acid]$_0$ = 250 mM. The different reactivities of singlet and triplet excited states of glyoxylic acid can provide an explanation to this enhancement. Under 1 atm O_2, the dissolved (triplet) diradical acts as a quencher that reduces the population of triplet excited state $^3GA^*$ and hydrogen abstraction by reaction R3 (Scheme 1). Therefore, reaction R2 (Scheme 1) is favored as the main producing channel for K$^{\bullet}$ through two reactions (R4 and R8) and tartaric acid by recombination R10. The presence of 1 atm O_2 enhances the production of HO_2 by reactions R7, R9, R11, R16 (Scheme 1) and through the reaction of HOOC$^{\bullet}$ with O_2 which eliminates $HO_2^{\cdot}/O_2^{\cdot-}$ quantitatively.[31]

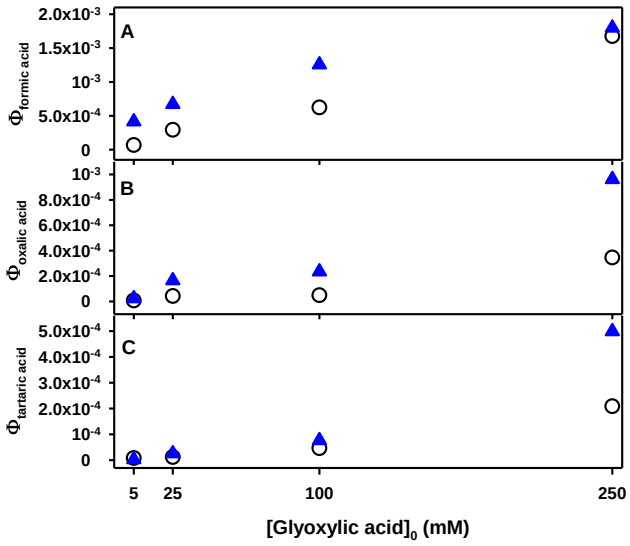

Figure S6. Apparent quantum yields of formation for (A) formic acid, (B) oxalic acid, and (C) tartaric acid vs initial [glyoxylic acid]$_0$ during 2 h photolysis ($\lambda \geq 305$ nm) in electrolytes under (black ○) 1 atm N_2(g) or (blue ▲) 1 atm O_2(g).

References

(1) Guzman, M. I.; Colussi, A. J.; Hoffmann, M. R. Photoinduced oligomerization of aqueous pyruvic acid. *J. Phys. Chem. A* **2006**, *110*, 3619-3626.

(2) Saxena, P.; Hildemann, L. M. Water absorption by organics: Survey of laboratory evidence and evaluation of UNIFAC for estimating water activity. *Environ. Sci. Technol.* **1997**, *31*, 3318-3324.

(3) Jang, M.; Czoschke, N. M.; Northcross, A. L. Atmospheric Organic Aerosol Production by Heterogeneous Acid-Catalyzed Reactions. *ChemPhysChem* **2004**, *5*, 1646-1661.

(4) Kawamura, K.; Imai, Y.; Barrie, L. A. Photochemical production and loss of organic acids in high Arctic aerosols during long-range transport and polar sunrise ozone depletion events. *Atmos. Environ.* **2005**, *39*, 599-614.

(5) Kawamura, K.; Yasui, O. Diurnal changes in the distribution of dicarboxylic acids, ketocarboxylic acids and dicarbonyls in the urban Tokyo atmosphere. *Atmos. Environ.* **2005**, *39*, 1945-1960.

(6) Schöne, L.; Herrmann, H. Kinetic measurements of the reactivity of hydrogen peroxide and ozone towards small atmospherically relevant aldehydes, ketones and organic acids in aqueous solutions. *Atmos. Chem. Phys.* **2014**, *14*, 4503-4514.

(7) Sorensen, P. E.; Bruhn, K.; Lindelov, F. Kinetics and equilibria for the reversible hydration of the aldehyde group in glyoxylic acid. *Acta Chem. Scand. A* **1974**, *28*, 162-168.

(8) Plath, K. L.; Axson, J. L.; Nelson, G. C.; Takahashi, K.; Skodje, R. T.; Vaidaa, V. Gas-phase vibrational spectra of glyoxylic acid and its gem diol monohydrate. Implications for atmospheric chemistry. *React. Kinet. Catal. Lett.* **2009**, *96*, 209-224.

(9) Harvey, H. W. *The Chemistry and Fertility of Sea Waters*, 2nd ed.; Cambridge University Press: New York, NY, U.S.A., 1957.

(10) Noziere, B.; Dziedzic, P.; Córdova, A. Products and kinetics of the liquid-phase reaction of glyoxal catalyzed by ammonium ions (NH_4^+). *J. Phys. Chem. A* **2008**, *113*, 231-237.

(11) Guzmán, M.; Hoffmann, M.; Colussi, A. Photolysis of pyruvic acid in ice: Possible relevance to CO and CO_2 ice core record anomalies. *J. Geophys. Res.-Atmos.* **2007**, *112*, D10123.

(12) Rincon, A. G.; Guzman, M. I.; Hoffmann, M. R.; Colussi, A. J. Optical absorptivity versus molecular composition of model organic aerosol matter. *J. Phys. Chem. A* **2009**, *113*, 10512-10520.

(13) Manahan, S. E. *Environmental Chemistry*, 9th ed.; CRC press: Boca Raton, FL, U.S.A., 2010.

(14) Zhou, R.; Guzman, M. I. CO_2 reduction under periodic illumination of ZnS. *J. Phys. Chem. C* **2014**, *34*, 11649-11656.

(15) Back, R. A.; Yamamoto, S. The gas-phase photochemistry and thermal decomposition of glyoxylic acid. *Can. J. Chem.* **1985**, *63*, 542-548.

(16) Leermakers, P. A.; Vesley, G. F. The photochemistry of α-keto acids and α-keto esters. I. Photolysis of pyruvic acid and benzoylformic acid. *J. Am. Chem. Soc.* **1963**, *85*, 3776-3779.

(17) Griffith, E. C.; Carpenter, B. K.; Shoemaker, R. K.; Vaida, V. Photochemistry of aqueous pyruvic acid. *P. Natl. Acad. Sci. U.S.A.* **2013**, *110*, 11714-11719.

(18) Li, K.; Stefan, M. I.; Crittenden, J. C. UV photolysis of trichloroethylene: Product study and kinetic modeling. *Environ. Sci. Technol.* **2004**, *38*, 6685-6693.

(19) SDBSWeb, http://sdbs.db.aist.go.jp; Accessed: 1/5/2016.

(20) Defoin, A.; Defoin-Straatmann, R.; Hildenbrand, K.; Bittersmann, E.; Kreft, D.; Kuhn, H. J. A new liquid phase actinometer: quantum yield and photo-CIDNP study of phenylglyoxylic acid in aqueous solution. *J. Photochem.* **1986**, *33*, 237-255.

(21) Görner, H.; Kuhn, H. J. Photodecarboxylation of phenylglyoxylic acid: Influence of para-substituents on the triplet state properties. *J. Chem. Soc. Perk. T. 2* **1999**, 2671-2680.

(22) Engel, P. S. Photochemistry of dibenzyl ketone. *J. Am. Chem. Soc.* **1970**, *92*, 6074-6076.

(23) Robbins, W. K.; Eastman, R. H. Photodecarbonylation in solution. I. Quantum yields and quenching results with dibenzyl ketones. *J. Am. Chem. Soc.* **1970**, *92*, 6076-6077.

(24) Rincon, A. G.; Guzman, M. I.; Hoffmann, M. R.; Colussi, A. J. Thermochromism of model organic aerosol matter. *J. Phys. Chem. Lett.* **2009**, *1*, 368-373.

(25) Schweitzer, F.; Magi, L.; Mirabel, P.; George, C. Uptake Rate Measurements of Methanesulfonic Acid and Glyoxal by Aqueous Droplets. *J. Phys. Chem. A* **1998**, *102*, 593-600.

(26) Hastings, W. P.; Koehler, C. A.; Bailey, E. L.; De Haan, D. O. Secondary Organic Aerosol Formation by Glyoxal Hydration and Oligomer Formation: Humidity Effects and Equilibrium Shifts during Analysis. *Environ. Sci. Technol.* **2005**, *39*, 8728-8735.

(27) Wasa, T.; Musha, S. Polarographic Behavior of Glyoxal and Its Related Compounds. *Bull. Univ. Osaka Prefect. Ser. A* **1970**, *19*, 169-180.

(28) Massari, J.; Tokikawa, R.; Medinas, D. B.; Angeli, J. P. F.; Di Mascio, P.; Assunção, N. A.; Bechara, E. J. H. Generation of singlet oxygen by the glyoxal–peroxynitrite system. *J. Am. Chem. Soc.* **2011**, *133*, 20761-20768.

(29) Maker, P. D.; Niki, H.; Savage, C. M.; Breitenbach, L. P. Fourier transform infrared spectrometric determination of gaseous performic acid. *Anal. Chem.* **1977**, *49*, 1346-1347.

(30) De Filippis, P.; Scarsella, M.; Verdone, N. Peroxyformic acid formation: A kinetic study. *Ind. Eng. Chem. Res.* **2009**, *48*, 1372-1375.

(31) von Sonntag, C.; Schuchmann, H.-P. The elucidation of peroxyl radical reactions in aqueous solution with the help of radiation-chemical methods. *Angew. Chem. Int. Ed.* **1991**, *30*, 1229-1253.